HHS Public Access

Author manuscript

J Neural Eng. Author manuscript; available in PMC 2024 January 18.

Published in final edited form as:

J Neural Eng. ; 20(1): . doi:10.1088/1741-2552/acae08.

Fully Desktop Fabricated Flexible Graphene Electrocorticography (ECoG) Arrays

Jia Hu[1,*], **Ridwan Fayaz Hossain**[1,*], **Zahra S. Navabi**[1], **Alana Tillery**[2], **Michael Laroque**[1], **Preston D. Donaldson**[3], **Sarah L. Swisher**[3], **Suhasa B. Kodandaramaiah**[^,1,4,5]

[1]Department of Mechanical Engineering, University of Minnesota Twin Cities

[2]School of Medicine, Johns Hopkins University

[3]Department of Electrical and Computer Engineering, University of Minnesota Twin Cities

[4]Department of Biomedical Engineering, University of Minnesota Twin Cities

[5]Department of Neuroscience, University of Minnesota Twin Cities

Abstract

Flexible Electrocorticography (ECoG) electrode arrays that conform to the cortical surface and record surface field potentials from multiple brain regions provide unique insights into how computations occurring in distributed brain regions mediate behavior. Specialized microfabrication methods are required to produce flexible ECoG devices with high-density electrode arrays. However, these fabrication methods are challenging for scientists without access to cleanroom fabrication equipment. Here we present a fully desktop fabricated flexible graphene ECoG array. First, we synthesized a stable, conductive ink via liquid exfoliation of Graphene in Cyrene. Next, we established a stencil-printing process for patterning the graphene ink via laser-cut stencils on flexible polyimide substrates. Benchtop tests indicate that the graphene electrodes have good conductivity of ~ 1.1×10^3 S·cm^{-1}, flexibility to maintain their electrical connection under static bending, and electrochemical stability in a 15-day accelerated corrosion test. Chronically implanted graphene ECoG devices remain fully functional for up to 180 days, with average *in vivo* impedances of 24.72 ± 95.23 kΩ at 1 kHz. The ECoG device can measure spontaneous surface field potentials from mice under awake and anesthetized states and sensory stimulus-evoked responses. The stencil-printing fabrication process can be used to create Graphene ECoG

[^]**Send manuscript correspondence to:** Suhasa B. Kodandaramaiah, Department of Mechanical Engineering, University of Minnesota, Twin Cities, **Address:** 111 Church St SE, Room 303, Minneapolis, MN 55455, suhasabk@umn.edu.

[*]Equal Contribution

AUTHOR CONTRIBUTIONS

SBK conceived the overall project. JH, RFH, AT, and SBK conceptualized the devices. JH developed the electrode array designs, laser-cut stencil technique, implant, and electrode interface. JH also designed and performed the *in vivo* experiments, surgical implantation, and data analysis with the help of ZN. RFH developed the recipe for the graphene inks and characterized the properties. RFH performed the electrical & material characterization and analysis. RFH also engineered and developed the stencil fabrication process of the ECoG electrode array and cleanroom fabrication of the test samples. JH and RFH performed the electrode bending test. PDD carried out CV and EIS experiments with the help of RFH and JH. ML designed and built the spin coater. JH, RFH, PDD, and SBK wrote the paper. All authors revised and contributed to the final manuscript.

INSTITUTIONAL APPROVAL

All animal experiments described in this paper were approved by the University of Minnesota's Institutional Animal Care and Use Committee (IACUC).

COMPETING INTERESTS

The authors declare no competing interests.

devices with customized electrode layouts within 24 hours using commonly available laboratory equipment.

INTRODUCTION

Simultaneous neural computations occurring in many brain regions, and the interactions between these regions, mediate behavior [1]–[3]. Disruptions to these interactions are an indicator of neurological disorders such as Parkinson's disease [4] and traumatic brain injury [5]. Minimally invasive electrocorticography (ECoG) electrode arrays have been used to measure surface field potential generated by neural activity from several distributed populations of neurons in the cortex [6]. Functionally, ECoG electrode arrays covering large brain regions need to be flexible to make adequate contact with the complex, convex surface of the brain [6], [7]. To this end, flexible, silicon substrate-based [8] and polymer substrate-based ECoG devices [7]–[19] have been developed. However, these devices were made using highly specialized micro- or nanofabrication techniques which require training and specialized fabrication equipment. Further, most neuroscience laboratories require rapid and flexible design alterations to adapt to various experimental contexts, which is hard to achieve with traditional microfabrication procedures. To simplify the fabrication procedure, inkjet printing conductive materials such as silver nanoparticle inks [9] and conductive polymer PEDOT:PSS ink [10] have been used to create flexible and reconfigurable ECoG electrode arrays. Currently, these approaches require expensive printers and still rely on specialized or microfabrication techniques to insulate the electrode [11].

This work introduces a fully-desktop fabricated, stencil-printed, flexible graphene ECoG electrode array, which is fabricated using commonly available equipment in neuroscience laboratories. Graphene has become an attractive material for fabricating neural interfaces [12]–[16] due to its high conductivity [17], flexibility [18], transparency [19], stability [20], and biocompatibility [18]. We first formulated a stable conductive ink based on exfoliating Graphene in Cyrene. The ink was then stencil-printed on a flexible polyimide substrate via laser-cut stencils. A similar procedure was applied to pattern a sacrificial layer of Pluronic, a triblock copolymer, for defining the exposed electrode pads. Lastly, a silicone elastomer insulation layer was coated on the electrodes using a custom-built, microprocessor-controlled spin-coater to create the functional ECoG electrode arrays. Most importantly, no aspect of the device fabrication needed access to specialized cleanroom facilities. The flexible Graphene ECoG devices exhibited excellent benchtop performance characteristics and *in vivo* recording capabilities in chronically implanted mice with surface field potentials recorded for up to 180 days. Using this methodology, the proposed devices can be fabricated within 24 hours and require a level of complexity and skill comparable to the assembly of tetrode devices [21].

RESULTS

Desktop fabricated flexible graphene ECoG electrodes

We sought to engineer a flexible graphene ECoG device that could be entirely fabricated using commonly available equipment in neuroscience laboratories. Previous work has been

done on stencil-printed graphene electronics [22]–[25], but fully desktop fabricated ECoG arrays implanted in mice have not been developed. First, the fabrication procedure required synthesizing a graphene ink to build the electrodes and retain electrical performance after chronic implantation. Secondly, we sought to establish a simple process for achieving reconfigurable electrode arrays for use in small animals. In this study, we used graphene exfoliated in Cyrene solvent to create a high-performance conductive ink that could be patterned on a polyimide (PI) film using a stencil-printing technique (Fig. 1a).

The overall fabrication procedure is shown in Fig. 1a. In the first step, two stencils were created using a desktop laser cutter; one stencil for patterning the graphene electrodes, and the second for patterning the Pluronic sacrificial layer that defined the electrode pads (Fig. 1a. i). The desktop laser cutter achieved a minimum inter-electrode (center to center) distance of ~ 400 μm. To reliably create isolated electrodes without any spurious interconnects, we used the minimum inter-electrode distance (center to center) of ~500 μm in the stable design with electrode trace width of ~200 μm (Fig. 1b, c). This inter-electrode distance (500 μm) depended on the laser power and cutting speed of the laser cutter, which was experimentally optimized (S.Fig. 1).

The first laser-cut stencil was overlaid on a flexible PI film, followed by drop-casting graphene ink to pattern the electrode arrays (Fig. 1a. ii). After drop-casting, the PI film with the stencil was annealed at a low temperature of ~ 100 °C to evaporate the excess Cyrene solvent. Then, the stencil was stripped, and the electrode array was annealed at a high temperature of ~ 300 °C (Fig. 1c). Once cooled to room temperature, the second stencil, for patterning the Pluronic sacrificial layer was overlaid on the substrate (Fig. 1a. iii). A fine paintbrush was used to apply Pluronic on the electrode pads through the second stencil (Fig. 1a. iii). After removing the stencil, the Pluronic layer was allowed to solidify overnight (Fig. 1c. iii). The graphene electrode array was then spin-coated with diluted silicone elastomer (PDMS) to create the insulating layer. Once the elastomer was cured, the electrode array was gently rinsed in warm water to remove the Pluronic sacrificial layer covering the electrode pads, resulting in an PDMS-insulated electrode array with exposed electrode pads with an average diameter of ~ 300 μm for interfacing the brain. The ECoG array also contains 16 electrode sites for interfacing with a printed circuit board (PCB) (S. Fig. 1a). Once the electrode arrays were fabricated, they were integrated into a 3D printed window frame adapted from our previous work [9], [26], [27]. The PCB interface was bonded to the ECoG array using conductive epoxy (S. Fig. 2a) and mechanically reinforced using a custom 3D printed clamp (Fig. 1d, e). The fabrication procedure relied entirely on common equipment such as a laser cutter and stereolithographic 3D printers, ubiquitous in nearly every university maker space. The electrode annealing was performed using a laboratory hotplate. Spin-coating was performed using a homebuilt microprocessor-controlled spinner (S. Fig. 5), but off-the-shelf low-cost speed-controllable spin coaters under $1000 can also serve the purpose.

Formulation of graphene inks and material characterization

We formulated three graphene inks for stencil fabrication by exfoliating graphene in Cyrene, Dimethylformamide (DMF) [28]–[31], and Cyclohexanone/Terpineol (C/T) [18],

[32], [33] solvents, using a top-down liquid-phase exfoliation (LPE) technique through ultra-sonication (see Methods for details). graphene inks in DMF and C/T have already been used in optoelectronic, photovoltaic, and biomedical applications [18], [29]–[34]. More recently, Cyrene demonstrated near-ideal physical properties for graphite exfoliation and the production of graphene dispersions [35]. For a sonication time of 2 hours, Graphene exfoliated in Cyrene resulted in drop-cast films with sub-micrometer surface flakes, whereas graphene exfoliated in DMF and C/T ink produced rougher films with much larger surface clusters (Fig. 2a). As shown in S.Figure 6, the Raman spectroscopy was performed on spin-cast films from the three ink samples. The I_d/I_g ratio for highly disordered graphitic films like those generated from annealed graphene flakes increases with crystallite (i.e. flake) size [36]. The I_d/I_g ratio for the Cyrene-exfoliated graphene sample is the lowest, indicating it has the least average distance between defects (< 1 nm), and that this sample is composed of the smallest flakes of the three inks, which were all annealed into a mainly sp^2 amorphous carbon structure [37]. Flake size is a determinant of the overall packing density, with a smaller flake size enhancing the inter-platelet connectivity, resulting in higher conductivity [18]. Further, smaller flake sizes are desirable for uniform patterning through stencils or inkjet printing if needed [18], [22]. The thickness of the drop-cast graphene inks were measured with a surface profiler to be 5.84 μm for Cyrene+Gr, 12.93 μm for C/T+EC+Gr, and 8.08 μm for DMF+EC+Gr (S. Fig. 7).

We next assessed the current-voltage characteristics of the three graphene films at room temperature (Fig. 2b). At 0.5 V, the current was measured to be ~ 61 mA for Cyrene+Gr,~ 1.1 mA for DMF+EC+Gr, and ~ 0.2 mA for C/T+EC+Gr. Following the calculation in the method session, this finding corresponds to the highest conductivity of the Cyrene ink sample (~ 1.1×10^3 $S \cdot cm^{-1}$). These results indicated that Cyrene was an adequate solvent for formulating the exfoliated graphene ink. The small flake size and high conductivity of Cyrene+Gr indicate its suitability for inkjet printing of electrodes [38] and as such, further experiments in this work involved devices made using graphene exfoliated in Cyrene.

Benchtop characterization of stencil fabricated graphene ECoG electrode arrays.

Cyclic voltammetry (CV) was used to evaluate the electrochemical stability of graphene electrodes [39]. The CV of the graphene electrode (n = 1) was measured at potentials with scan rates ranging from 50 mV/s to 1000 mV/s. According to the shape of the plotted curves, both double-layer capacitance and pseudo-capacitance exist in the electrode (Fig. 2e) [40]. The capacitance value was extracted from the current (at 400 mV) vs. scan rate from the CV curve where the linear fit slope approximates the capacitance and was calculated to be ~ 10 nF at 400 mV.

Electrochemical impedance spectroscopy (EIS) measured over a frequency range of 1 Hz to 10 kHz (Fig. 2c) was performed on a graphene ECoG device with 15 functional electrodes (We used a sample of 15 electrodes from one device to ensure the fabrication condition remains the same). The phase angle shows the typical capacitive behavior (near 80°) at 20 Hz but gradually becomes more resistive at higher frequencies (Fig. 2d). At high frequencies ranging from 1 kHz to 10 kHz, the relatively low impedance magnitudes are attributed to the stray capacitance and the Ohmic resistance of the electrolyte solution and interconnect [41].

The EIS of the stencil-printed graphene electrode presents similar impedance characteristics as a previously reported ECoG array of monocrystalline graphene layers [14].

To evaluate the durability of the PDMS insulator and stability of graphene electrodes, we used ECoG arrays with 16 exposed electrode pads as the controls and the ECoG arrays with 16 electrode pads fully encapsulated with PDMS as the test device in accelerated corrosion test (Fig. 2f). Accelerated corrosion tests are typically used to evaluate the durability of devices by maintaining the devices in a 1X PBS solution for extended durations at high temperatures (60°C). Such tests simulate a fivefold acceleration in device degradation as compared to devices kept at physiological temperatures [42]. Based on these metrics, we performed accelerated corrosion tests lasting 15 days to evaluate the impedances for a projected 75-day period. At the end of the 15-day accelerated corrosion tests, the electrodes had an average impedance of 6.49 ± 4.16 kΩ (n = 16) while devices fully encapsulated with PDMS all had impedances > 1 MΩ. These results indicate that the potential lifetime of the electrodes is at least 75 days at body temperature of 37°C.

The planar ECoG electrode array is typically bent to conform to the mouse's convex dorsal cortex with an approximate radius of curvature of 12 mm [26]. Therefore, it is important to investigate the relationship between the electrode impedance and the bending radii of curvature. The impedances of 9 identical, 10 mm long, straight, graphene electrodes were measured at 1 kHz while the electrodes were placed on a flat surface and then again when bent at various radii of curvature using a custom measurement rig (S. Fig. 3). No significant difference in the electrode impedance magnitudes could be found between electrodes placed on a flat surface and those at different radii of curvature (14 mm to 6 mm) (Fig. 3g). Thus, the graphene electrodes patterned on the flexible PI substrates can be bent to conform to the dorsal cortical surface of the mouse brain with minimal effect on the electrode impedance.

In vivo experiments

The graphene ECoG devices were implanted on 4 mice to evaluate *in vivo* recording capabilities. The overall array dimensions were ~ 9 mm x 4 mm, covering most of the sensory cortex areas bilaterally (Fig. 4b). Representative microscope images of one such implanted mouse taken on days 22 and 182 after implantation are shown in Fig. 3a. No visible neuroimmune response such as Dural thickening and tissue encapsulation in these devices could be found. Most of the inner surface of the implant was covered by a PDMS insulation layer (Fig. 1c). PDMS itself is a biocompatible material for long-term cranial implants [43]. The longest duration of implantation assessed was 21 weeks. The impedances of the electrodes were periodically measured throughout the implantation (Fig. 3b). Across 4 mice, 61 electrodes (out of 64) remained functional, with an average impedance magnitude of 24.72 ± 95.23 kΩ (n = 61) at 1 kHz. Three electrodes lost their connections on Mouse #1 at the measurement on day 10. Based on previous work describing a graphene ECoG device with similar electrode sizes, the impedance of functional ECoG electrodes was expected to be lower than 600 kΩ at 1 kHz [15]. The average electrode impedances of all four devices evaluated in this study remained less than 600 kΩ throughout implantation (n = 61/64 electrodes). Therefore, our graphene electrode arrays can be used for chronic *in vivo* studies.

ECoG recordings were performed in head-fixed mice while fully awake and under Ketamine-anesthesia to demonstrate the functional use of the graphene ECoG devices. The raw recordings obtained from all 16 electrodes in both states are shown in Figure. 3c. Consistent with previous observations [44]–[46], induction of the anesthetized state via Ketamine resulted in low-frequency oscillations at the delta frequency (0.5 – 4 Hz) throughout the cortex (Fig. 3c). These delta oscillations had signal peak-to-peak amplitudes of approximately 500 μV, much higher than the awake state's amplitude of ~ 200 μV (Fig. 3c). The spectrogram in Figure. 3d also presents a higher signal power density at 0.5 – 4 Hz at the anesthetized state, matching the power spectral density (PSD, Fig. 3e). The result indicates that all 16 channels of the device were functional to measure brain activity.

Furthermore, the graphene ECoG devices demonstrated the ECoG recordings of stimuli-evoked brain activity in response to sensory stimuli. The stimuli were brief puffs of air (100 ms) given to the right whiskers of mice at randomized intervals during the awake state under head-fixation (Fig. 4a). Whisking and motor response were both observed in the experiments in response to the stimuli. Broad activation of most of the cortex in response to the stimuli was also observed and possibly caused by the startle response (Fig. 4c). Channels 1 and 16 were individually located at the contralateral and ipsilateral sensory cortices (S1) (Fig. 4b). Channel 1 showed higher signal amplitudes of negative peak N1 and positive peak P2 than channel 16 (Fig. 4d). Three animals (Mouse #1, Mouse #2, and Mouse #4) were used to analyze the signal difference between Channels 1 and 16. As shown in Figure. 4e and f, the average N1 values in electrodes 1 vs. 16 were - 83.60 ± 23.16 μV vs. - 48.20 ± 12.29 μV ($p < 0.001$, *t-test*) on all three mice; the average P2 values in electrode 1 vs. 16 were 48.64 ± 19.96 μV vs. 34.34 ± 11.28 μV ($p < 0.05$, *t-test*) on all three mice. Both N1 and P2 values measured by electrode 1, placed on the left somatosensory cortex (contralateral to the right whisker experienced air-puff stimulation), are significantly higher in amplitude than electrode 16, located on the right somatosensory cortex. Thus, the graphene ECoG electrode arrays successfully captured the evoked response to the lateral right whisker air-puff stimulation. These results are consistent with previous work done in our group [27], [47].

DISCUSSION

Here, we demonstrated for the first time a fully desktop-fabricated ECoG electrode array which we implanted on the rodent dorsal cortex for neurophysiological recording. The highly stable graphene ink formulated by exfoliating graphene in a biocompatible solvent Cyrene [48] demonstrated a high conductivity ~ 1.1×10^3 S·cm^{-1}. Mechanical bending tests showed no significant change in electrode impedance at a flat surface and various radii of curvature ranging from 14 mm to 6 mm. Fully functional devices and the encapsulation of PDMS insulation were highly stable even under the accelerated aging environment, maintaining an average impedance of ~ 6.49 ± 4.16 kΩ on day 15. Furthermore, the electrodes remained functional with an average impedance magnitude of 24.72 ± 95.23 kΩ (1 kHz) throughout the implantation. Thus, our graphene ECoG arrays provide robust neural interfaces that can be applied for chronic electrophysiology studies in mice.

To our knowledge, all the existing micrometer-scale ECoG devices are fully or partially fabricated using microfabrication or specialized techniques [42], [43], [49]–[56], resulting in high cost and low accessibility to neuroscience laboratories. In our method, the stencils determining the layout of the electrodes can be rapidly reconfigured using CAD tools and fabricated using desktop laser-cutters available in most university fabrication shops. The graphene ink can be formulated using standard lab equipment, and the patterned electrodes can be sintered on a laboratory hotplate. The insulation layer can be deposited by a homebuilt, microcontroller-based spinner or a low-cost off-the-shelf spin coater. We have created the first fully desktop fabricated, flexible micrometer-scale ECoG array that can be chronically implanted in mice. These results point a way forward for creating robust, open-source, flexible neural interfaces that can be widely used in basic and translational neuroscience research.

Some limitations and concerns of the electrode characterization tests and results should be clarified and discussed. First, the conductivity of the Cyrene graphene electrode was measured to be ~1.1×10^5 S/m, which is sufficient for use in neural probes, and is comparable to a PEDOT:PSS composite material ($3.23 \pm 0.75 \times 10^2$ S/m) from a previous study [57]. However, the conductivity of the stencil-printed multilayer graphene electrode (~1.1×10^5 S/m) is not comparable with monolayer graphene ($1.46 \pm 0.75 \times 10^6$ S/m) synthesized by chemical vapor deposition [58]. To improve the conductivity of the ECoG electrode made by our desktop fabrication method, new conductive inks, such as inkjet printable gold nanoparticle ink (8.0×10^6 S/m), can be considered [59]. Secondly, for conducting the accelerated corrosion test, we used a 50 ml centrifuge tube that could only fit 2 devices with a total of 32 electrodes (one functional device consisting of partially PDMS-encapsulated graphene electrodes to evaluate the stability of the graphene electrodes and one device consisting of fully PDMS-encapsulated graphene electrodes to evaluate the durability of the PDMS insulation layer). Future studies with improved Graphene ECoG arrays can be evaluated with larger samples sizes. Further, the decrease in impedance values of graphene electrodes from day 0 to day 5 (Fig. 2f) might indicate vapor penetration through the PDMS insulation, which is water-repellent but permeable to water vapor [60]. To resolve this possible vapor penetration, alternate flexible insulation material, such as SU-8 [52], can be used instead. Thirdly, the impedance values (24.72 ± 95.23 kΩ at 1 kHz, n = 61) of the implanted ECoG devices have a high variability. One possible cause of this variability is the stencil printing fabrication method, where drop-casting the conductive ink through the laser-cut stencil made the thickness of the graphene electrodes difficult to control. To mitigate this, spin-coated or drop-casted PEDOT:PSS with smaller particle size can be explored in the future to reduce the impedance variability, as demonstrated previously [61].

We also identified some limitations to the proposed approach. First, the minimum feature size is limited by the resolution of the desktop laser cutter to create the stencils. Our ECoG devices with an inter-electrode (center to center) distance of ~ 500 μm could be reliably patterned using the laser cutter, which limits the overall number and density of electrodes incorporated within a device. Second, the graphene ink needs to be annealed at high temperatures (> 300°C), limiting the type of substrate materials that can be used for supporting the graphene electrodes. As an alternative, photonic sintering can be used

instead of thermal annealing, which would allow the use of substrate materials with low melting point, including transparent polymers such as polyethylene terephthalate (PET). Patterning electrodes on transparent polymers creates devices for simultaneous imaging and ECoG recording [11] which currently require specialized equipment to fabricate [49]. Our desktop-fabricated, stencil printing method has not yet been demonstrated on transparent graphene ECoG, but off-shelf transparent conductive PEDOT:PSS ink [8] can be a potential alternative for making fully transparent ECoG.

We would also like to note that while the fabrication procedure described here is well established in our group, direct implementation of the same may take some degree of optimization in the end-user labs. In our hands, synthesis of the ink takes 27 hours, including a 24-hour waiting period, and the ink can be stored and used for at least 2 months. One-time fabrication of 24 laser-cut masks takes 15 minutes, followed by 12 hours, including an 8-hour waiting period, for fabrication and assembly of 2–3 devices. It is especially critical to carefully perform the Pluronic deposition step of the fabrication procedure, which can result in failure due to misalignment of the Pluronic sacrificial layer and the graphene electrode pads. These are necessary considerations for achieving high-performance devices. It must be noted that laser-induced graphene [62] may be more efficient to pattern electrodes but the laser-induced graphene itself still requires specialized microfabrication methods which may not be accessible to all end user laboratories.

Several directions can be pursued in the future, building upon the graphene ECoG devices presented in this work. The size of the implant can be extended to much larger regions of the brain [26], [27] so that the whole visual cortex and motor cortex can be included for performing ECoG recording over most of the cortical surface of the mouse brain [11]. The low and stable impedance of the electrodes can be leveraged for precise cortical micro-stimulation [14]. Miniaturization of electronic interface circuits can also allow deployment in freely behaving animals, potentially combined with imaging instrumentation for simultaneously tracking large-scale calcium dynamics [27]. Further, graphene has shown utility in passive sensing of electrical potentials and functionalizing to highly sensitive biochemical sensing [63]. Overall, our method can be scaled to mass manufacturing of flexible graphene-based biosensors at a low cost with a myriad of applications in biological sensing, such as electrocardiography [64], electromyography [65], and peripheral nerve interfacing [66].

METHODS

Graphene inks formulation:

The graphene inks were formulated by bath ultra-sonication of graphene powder, which was ground using a mortar and pestle from a graphite rod (496561, Sigma Aldrich), in a mixture of Cyclohexanone and Terpineol (C/T) (398241 and 814759, Sigma Aldrich) at a ratio of 7:3, DMF(319937, Sigma Aldrich), and Cyrene (807796, Sigma Aldrich). An initial concentration of Ethyl Cellulose (EC) (EC 200646, Sigma Aldrich) at 2.5 wt% and 10 mg/mL graphene powder were then added in 10 mL C/T and DMF, treated for 2 hours in the Branson Bath Sonicator (CPX2800, Fisher Scientific) at 30 °C. No EC was added to the Cyrene ink as it produces excess bubbles resulting in bad drop casting. All three

dispersions were kept idle for 24 hours to precipitate the larger particles, which left pale gray precipitation at the bottom of the vials. The supernatant (~ 8 mL) inks were extracted and stored in clean vials.

Graphene sample preparation for Electrical Measurement:

To carry out the initial electrical characterization of the graphene inks, high integrity metal contacts composed of silver (*Ag*) were first patterned with photolithography and deposited with an e-beam evaporator on the PI film, followed by drop-casting of 0.5 mL graphene ink in a rectangular area of 10.5 mm x 2 mm using a stencil (S.Fig. 4). The sample was annealed at 350 °C for 90 minutes. A probe station with parameter analyzer (B1500A, Agilent Technologies) was used to conduct 2-point-probe voltage-controlled measurements and data extraction to evaluate the current-voltage characteristics of three graphene films (Fig. 2b). The current density (A/cm^2) was calculated from the measured current values (A) (Fig. 2b) divided by the cross-session area of the sample of 1.17×10^{-4} cm^2 (sample width of 2 mm × sample thickness of 5.84 μm of Cyrene graphene). The electric field (V/cm) was defined as applied voltage (V) (Fig. 2b) divided by the sample length of 1.05 cm. The conductivity (S/cm) of the graphene sample was calculated by dividing the current density (A/cm^2) by the electric field (V/cm).

Electrode array design and assembly:

Electrode array design: The layout of the graphene electrode array was rendered in computer-aided design software (SolidWorks 2021, Dassault) (Fig. 1c). The center-to-center distances between 2 neighboring electrode pads ranged from ~ 600 μm to 1 mm. The overall layout of the electrode array was designed to cover an area of ~ 9 mm long, extending bilaterally, with a width of ~ 4 mm posterior to Bregma (Fig. 4b). Electrodes 1–3 and 14–16 were in the primary sensory cortex (S1); electrodes 4 and 13 were located in the visual cortex (V1); electrodes 5–6 and 11–12 were located in the primary motor cortex (M1/M2), and 7–10 were located in Retrosplenial cortex (RSC).

Laser-cut stencils: To fabricate the stencils, a piece of 50 μm-thick insulating polyimide (PI) tape (High Temperature Tape, Bertech) with a size of 25.4 mm by 160 mm was adhered to a stainless-steel sheet and subsequently patterned by a CO_2 laser cutter (PLS6.140D, Universal System) (Fig. 1a). We tested the laser cutter's cutting precision on the PI tape and found that the inter-electrode pitch (center to center distance) of ~ 500 μm with power settings of 10% and speed settings of 100% can consistently fabricate the stencils used in this study (S.Fig. 1b). The electrode via stencil was transferred to a polyimide film substrate using a scotch tape transfer method modified from previous work [67].

Graphene ink deposition: The graphene ink was manually drop-cast on the laser-cut mask and annealed at a high temperature (~ 350 °C) for 90 minutes. To evaporate the solvent completely, the hotplate temperature was ramped at ~ 10 °C/minute from 100 °C to 330 °C to evaporate the solvent completely. After annealing, the mask was carefully removed, leaving the patterned graphene channels on the polyimide film. A similar procedure was used to apply a sacrificial layer of Pluronic, a triblock copolymer, (F-127, Sigma Aldrich) after manually aligning the electrode pad stencil to the graphene electrodes. The sample was

kept overnight at room temperature to solidify the Pluronic. Diluted Polydimethylsiloxane (PDMS) was spin-coated at 1500 rpm for 15s using a home-built desktop spin-coater (S.Fig. 5), then cured at 30 °C temperature for 15 minutes. For making the diluted PDMS, the tert-Butanol (471712, Sigma) was warmed at 45 °C and mixed with PDMS and SYLGARD 184 curing agent (761036, Sigma) at the weight ratio of 50:10:1. The Pluronic was rinsed away with a gentle flow of hot water at 45 – 60 °C to expose the electrode pads. Then the sample was annealed again at 100 °C for 30 minutes.

Implant assembly: The graphene ECoG device is an assembly of four major components: the stencil fabricated ECoG array, a 3D printed cranial window frame, a flexible printed circuit board (PCB) connector, and a 3D printed reinforcement clamp. The cranial window frame and the reinforcement clamps were 3D-printed using a stereolithography 3D printer (Form 2, Formlabs). The PCB connector was custom-designed in Eagle (Autodesk Inc.) and fabricated by an online PBC manufacturer (PCBWay.com). To assemble the device, the ECoG electrode array was first bonded to the gold soldering pads on the flexible PCB connector using a conductive adhesive (8331 Silver Epoxy Adhesive, MG Chemical) (S. Fig. 2) by applying it manually with a sharp object. The interface was further mechanically reinforced using the 3D-printed clamp and followed by encapsulation with clear epoxy adhesive (Scotch-Weld Epoxy Adhesive DP100 Plus, 3M). The recording area of the stencil fabricated graphene electrode arrays was bonded to a 3D printed cranial window frame using epoxy adhesive (DP1000 Plus Clear, 3M) adapted from our previous work [26], [27] to realize the device illustrated in Fig. 1e. The cranial window defined a total recording area of ~ 4 mm x 9 mm, with a radius of curvature of 10 mm, to allow conformal implantation over the dorsal cortex immediately posterior to Bregma (Fig. 4b). A fully assembled device has a mass of ~ 1.3 g.

Benchtop testing of fully assembled devices:

CV (Fig. 2b), EIS (Fig. 2c, d), and accelerated corrosion tests (Fig. 2f) were performed on fully assembled graphene ECoG devices. EIS and CV measurements were conducted using a potentiostat (1010E, Gamry Instruments), with an Ag/AgCl reference electrode (Gamry Instruments) and a platinum wire as a counter electrode (1.0 mm diameter, Premion, 99.997%, Alfa Aesar) in room temperature 1X Phosphate Buffered Saline solution (D1408 PBS 10X, Sigma-Aldrich). EIS was performed with a 50 mV excitation voltage from 10 kHz to 1 Hz. Ten measurements were taken per decade. The CV was performed at varying scan rates from 50 – 1000 mV/s, with voltage limits set at ± 0.75 V vs. the open circuit potential.

The accelerated corrosion test was performed [68] by immersing 2 ECoG devices (one device has 16 exposed electrode pads, and one device has 16 fully PDMS-capsulated electrode pads) into 1X Phosphate-buffered saline (D1408 PBS 10X, Sigma-Aldrich) at an elevated temperature of 60 °C which is equivalent to a five-fold accelerated corrosion process at body temperature of 37 °C [42]. Impedances of the device were measured using the interface board (RHD2000, Intan Technologies) at 1 kHz daily for 2 weeks.

Bending testing was conducted by creating 9 straight, parallel graphene electrodes using the same ECoG stencil printing technique. To mimic various degrees of bending after

implantation, the electrodes were placed on a flat surface and custom-built acrylic structures (S.Fig. 3) with radii of curvature of 6 mm, 8 mm, 10 mm, 12 mm, and 14 mm, while their impedance was measured using the interface board (RHD2000, Intan Technologies Inc.) at 1 kHz.

Surgical implantation:

All animal experiments were approved by the University of Minnesota Intuitional Animal Care and Use Committee (IACUC). 9 C57BL/6 mice (5 males and 4 females) at the age of 12–30 weeks were used in this study. Initially, 5 mice were implanted with the graphene ECoG devices during the optimization of the electrode layout and overall device design. Mice were housed in a 14hr light/10hr dark cycle in rooms maintained at 20–23 °C and 30–70% relative humidity. Mice had ad libitum access to food and water. Mice were given preemptive doses of 2mg/kg of sustained-release buprenorphine (Buprenorphine SR-LAB, ZooPharm) and 2 mg/kg of meloxicam for analgesia and preventing brain inflammation, respectively. Mice were anesthetized 30–60 minutes after the initial analgesia dosage using 1–5% isoflurane anesthesia in Oxygen. Eye ointment (Puralube, Dechra Veterinary Products) was applied to the eyes. The scalp was shaved and cleaned. Once the mice were fixed in a stereotax (900LS, Kopf), the scalp was sterilized by repeatedly scrubbing Betadine and 70% Ethanol solution (3 times). Next, the scalp was removed using surgical scissors. The tissue and fat under the scalp were subsequently cleared using a micro curette (# 10080–05; Fine Science Tools). Partial temporalis muscle wrapping around the skull was carefully removed using a scalpel to expose the squamosal area. After drilling a ~ 300 μm-diameter hole on the squamosal suture, a stainless-steel bone screw (#FF000CE094, JI MORRIS Company) tied to a 26-gauge stainless-steel reference wire was tightened in the hole firmly. A large craniotomy was immediately performed using a high-speed dental drill following a rectangular path approximately 4 mm x 9 mm posterior to Bregma. After the drilling, the skull piece was removed from the dorsal cortex using two micro curettes holding its lateral edges. A gauze pad soaked in sterile saline was gently placed on the exposed brain to keep it moist.

The graphene ECoG device was sterilized by immersion in 70% Ethanol for 2 min and subsequently rinsed thoroughly with sterile saline. The periphery of the craniotomy was cleaned using a pointed cotton tip after removing the gauze pad. The window frame was gently placed on the exposed brain. Surgical adhesive (Vetbond, 3M) was applied around the edges of the window frame to bond the window frame to the skull. After the adhesive was cured, a customized waterjet-cut Titanium headplate was fastened on the implant with a #0–80 screw. The implant was cemented to the skull using opaque dental cement (Metabond, Parkell Inc.). Mice were transferred from the stereotax to a heated pad (catalog no. 72–0492; Harvard Apparatus) for recovery from the anesthesia and were transferred to a clean cage partially located on a warming pad once they were fully ambulatory. 2 mg/kg meloxicam was administrated twice per 24 hr for 72 hr post-surgery. Mice recovered for 7 days before any *in vivo* experiment.

In vivo electrophysiology:

In vivo electrode performance test: The impedances of electrodes in the implanted devices were measured periodically (up to 182 days). Animals were transferred from their home cage and affixed under anesthesia in a custom head-fixation device adapted from previous studies [26], [69]. Subsequently, the FPC connector on the amplifier was connected to the PCB connector of the ECoG device. Impedance measurements were acquired at 1 kHz.

Awake and anesthetized spontaneous recordings: Mice were head-fixed on the treadmill, and 4 minutes of spontaneous recordings were acquired when the animals were fully awake. All the signals were recorded through the RHD 2000 interface board at a sampling rate of 20 kHz. Mice were administrated a cocktail of Ketamine (100 mg/kg) and xylazine (10 mg/kg) while head-fixed. A heated pad was placed under the animal to maintain body temperature, and mice were supplemented with Oxygen. Once the animal was fully unresponsive to toe pinch stimulus, multiple 4-minute-long spontaneous recordings were acquired. Once fully recovered from anesthesia, mice were removed from the head fixation apparatus and transferred back to their home cage.

ECoG recordings in response to sensory stimuli: Stimulation applied to mice whiskers is a common way to study the evoked response in the somatosensory system [70]. Here, we used a lateral air-puff stimulation to test whether the implanted ECoG array can successfully measure the contralateral evoked response [27], [47]. To do so, brief air-puff stimuli of compressed air flow were applied to the right whiskers of head-fix mice through a blunt 24-gauge stainless steel needle. The needle guided the air-puff to stimulate the whiskers in the posterior-anterior direction (Fig. 4a). In each experimental session, each mouse received 24–30 air-puff stimuli with 100 ms duration. The inter-stimulus interval was randomized (8 to 10s) and controlled using a using a microcontroller (Arduino Uno, Adafruit) actuated solenoid valve.

Data analysis:

All the data, including electrode impedances and ECoG signals, were collected and converted using the interface board's software (RHD2000 interface, Intan Technologies Inc.). The raw ECoG signals were first down-sampled to a moving average of 2 kHz and low-pass filtered using an elliptic filter with a passband of 100 Hz. Custom scripts in MATLAB (MATLAB 2020b, MathWorks) were used to analyze and plot the data.

Supplementary Material

Refer to Web version on PubMed Central for supplementary material.

ACKNOWLEDGEMENTS

SBK and SLS acknowledge NINDS Award #R0NS111028. SBK acknowledges Brain Initiative Award R42NS110165. Parts of this work were carried out in the Characterization Facility, at the University of Minnesota, which receives partial support from the NSF through the MRSEC (Award Number DMR-2011401) and the NNCI (Award Number ECCS-2025124) programs. Portions of this work were conducted in the Minnesota Nano Center, which is supported by the National Science Foundation through the National Nanotechnology Coordinated Infrastructure (NNCI) under Award Number ECCS-2025124. We acknowledge Javier Garcia Barriocanal for assistance with the XRD measurements. PDD was supported by NSF IGERT Award DGE-1069104. Skylar Fausner

for assistance with animal preparation. We thank Skylar Fausner, Beatrice Gulner, and James Hope for useful comments and critiques of the paper.

Reference

[1]. TORRES I, “Human Behavior and the Developing Brain,” American Journal of Psychiatry, vol. 152, no. 4, 1995, doi: 10.1176/ajp.152.4.637-a.

[2]. Moustafa A, Computational Models of Brain and Behavior. 2017. doi: 10.1002/9781119159193.

[3]. West SL et al. , “Wide-Field Calcium Imaging of Dynamic Cortical Networks during Locomotion,” Cerebral Cortex, 2021, doi: 10.1093/cercor/bhab373.

[4]. Bijsterbosch JD et al. , “The relationship between spatial configuration and functional connectivity of brain regions,” Elife, vol. 7, 2018, doi: 10.7554/eLife.32992.

[5]. Cramer SW et al. , “Wide-field Calcium Imaging Reveals Widespread Changes in Cortical Connectivity Following Repetitive, Mild Traumatic Brain Injury in the Mouse,” bioRxiv, 2022.

[6]. Kim J, Lee M, Rhim JS, Wang P, Lu N, and Kim DH, “Next-generation flexible neural and cardiac electrode arrays,” Biomedical Engineering Letters, vol. 4, no. 2. 2014. doi: 10.1007/s13534-014-0132-4.

[7]. Khodagholy D. et al. , “NeuroGrid: Recording action potentials from the surface of the brain,” Nat Neurosci, vol. 18, no. 2, 2015, doi: 10.1038/nn.3905.

[8]. Rachinskiy I. et al. , “High-Density, Actively Multiplexed µECoG Array on Reinforced Silicone Substrate,” Frontiers in Nanotechnology, vol. 4, 2022, doi: 10.3389/fnano.2022.837328.

[9]. Donaldson PD, Ghanbari L, Rynes ML, Kodandaramaiah SB, and Swisher SL, “Inkjet-Printed Silver Electrode Array for in-vivo Electrocorticography,” in International IEEE/EMBS Conference on Neural Engineering, NER, 2019, vol. 2019-March. doi: 10.1109/NER.2019.8717083.

[10]. Donaldson PD and Swisher SL, “Transparent, Low-Impedance Inkjet-Printed PEDOT:PSS Microelectrodes for Multimodal Neuroscience,” Physica Status Solidi (A) Applications and Materials Science, 2022, doi: 10.1002/pssa.202100683.

[11]. Donaldson PD et al. , “Polymer skulls with integrated transparent electrode arrays for cortex-wide opto-electrophysiological recordings,” bioRxiv, p. 2021.11.13.468490, Jan. 2021, doi: 10.1101/2021.11.13.468490.

[12]. Ryu M. et al. , “Enhancement of Interface Characteristics of Neural Probe Based on Graphene, ZnO Nanowires, and Conducting Polymer PEDOT,” ACS Appl Mater Interfaces, vol. 9, no. 12, 2017, doi: 10.1021/acsami.7b02975.

[13]. Bourrier A. et al. , “Monolayer Graphene Coating of Intracortical Probes for Long-Lasting Neural Activity Monitoring,” Adv Healthc Mater, vol. 8, no. 18, 2019, doi: 10.1002/adhm.201801331.

[14]. Park DW et al. , “Electrical Neural Stimulation and Simultaneous in Vivo Monitoring with Transparent Graphene Electrode Arrays Implanted in GCaMP6f Mice,” ACS Nano, vol. 12, no. 1, 2018, doi: 10.1021/acsnano.7b04321.

[15]. Park DW et al. , “Graphene-based carbon-layered electrode array technology for neural imaging and optogenetic applications,” Nat Commun, vol. 5, 2014, doi: 10.1038/ncomms6258.

[16]. Kuzum D. et al. , “Transparent and flexible low noise graphene electrodes for simultaneous electrophysiology and neuroimaging,” Nat Commun, vol. 5, 2014, doi: 10.1038/ncomms6259.

[17]. Geim AK and Novoselov KS, “The rise of graphene,” Nat Mater, vol. 6, no. 3, 2007, doi: 10.1038/nmat1849.

[18]. Hossain RF, Deaguero IG, Boland T, and Kaul AB, “Biocompatible, large-format, inkjet printed heterostructure MoS 2-graphene photodetectors on conformable substrates,” NPJ 2D Mater Appl, vol. 1, no. 1, pp. 1–10, 2017.

[19]. Nair RR et al. , “Fine structure constant defines visual transparency of graphene,” Science (1979), vol. 320, no. 5881, 2008, doi: 10.1126/science.1156965.

[20]. Cristarella TC, Chinderle AJ, Hui J, and Rodríguez-López J, “Single-layer graphene as a stable and transparent electrode for nonaqueous radical annihilation electrogenerated chemiluminescence,” Langmuir, vol. 31, no. 13, 2015, doi: 10.1021/la5050317.

[21]. Voigts J, Siegle J, Pritchett DL, and Moore CI, “The flexDrive: An ultra-light implant for optical control and highly parallel chronic recording of neuronal ensembles in freely moving mice,” Front Syst Neurosci, no. MARCH 2013, 2013, doi: 10.3389/fnsys.2013.00008.

[22]. Hyun WJ, Secor EB, Hersam MC, Frisbie CD, and Francis LF, “High-resolution patterning of graphene by screen printing with a silicon stencil for highly flexible printed electronics,” Advanced Materials, vol. 27, no. 1, 2015, doi: 10.1002/adma.201404133.

[23]. Xu Y. et al. , “Screen-printable thin film supercapacitor device utilizing graphene/polyaniline inks,” Adv Energy Mater, vol. 3, no. 8, 2013, doi: 10.1002/aenm.201300184.

[24]. Yong K, Ashraf A, Kang P, and Nam S, “Rapid Stencil Mask Fabrication Enabled One-Step Polymer-Free Graphene Patterning and Direct Transfer for Flexible Graphene Devices,” Sci Rep, vol. 6, 2016, doi: 10.1038/srep24890.

[25]. Jabari E, Ahmed F, Liravi F, Secor EB, Lin L, and Toyserkani E, “2D printing of graphene: A review,” 2D Materials, vol. 6, no. 4. 2019. doi: 10.1088/2053-1583/ab29b2.

[26]. Ghanbari L. et al. , “Cortex-wide neural interfacing via transparent polymer skulls,” Nat Commun, vol. 10, no. 1, 2019, doi: 10.1038/s41467-019-09488-0.

[27]. Rynes ML et al. , “Miniaturized head-mounted microscope for whole-cortex mesoscale imaging in freely behaving mice,” Nat Methods, vol. 18, no. 4, 2021, doi: 10.1038/s41592-021-01104-8.

[28]. Htwe YZN, Abdullah MK, and Mariatti M, “Optimization of graphene conductive ink using solvent exchange techniques for flexible electronics applications,” Synth Met, vol. 274, 2021, doi: 10.1016/j.synthmet.2021.116719.

[29]. Alamri AM, Leung S, Vaseem M, Shamim A, and He J-H, “Fully inkjet-printed photodetector using a graphene/perovskite/graphene heterostructure,” IEEE Trans Electron Devices, vol. 66, no. 6, pp. 2657–2661, 2019.

[30]. Casaluci S, Gemmi M, Pellegrini V, di Carlo A, and Bonaccorso F, “Graphene-based large area dye-sensitized solar cell modules,” Nanoscale, vol. 8, no. 9, pp. 5368–5378, 2016. [PubMed: 26883743]

[31]. Silva M, Pinho IS, Covas JA, Alves NM, and Paiva MC, “3D printing of graphene-based polymeric nanocomposites for biomedical applications,” Functional Composite Materials, vol. 2, no. 1, pp. 1–21, 2021.

[32]. Fang Y, Hester JGD, Su W, Chow JH, Sitaraman SK, and Tentzeris MM, “A bio-enabled maximally mild layer-by-layer Kapton surface modification approach for the fabrication of all-inkjet-printed flexible electronic devices,” Sci Rep, vol. 6, 2016, doi: 10.1038/srep39909.

[33]. Secor EB, Prabhumirashi PL, Puntambekar K, Geier ML, and Hersam MC, “Inkjet printing of high conductivity, flexible graphene patterns,” J Phys Chem Lett, vol. 4, no. 8, pp. 1347–1351, 2013. [PubMed: 26282151]

[34]. Michel M, Biswas C, and Kaul AB, “High-performance ink-jet printed graphene resistors formed with environmentally-friendly surfactant-free inks for extreme thermal environments,” Appl Mater Today, vol. 6, pp. 16–21, 2017.

[35]. Pan K. et al. , “Sustainable production of highly conductive multilayer graphene ink for wireless connectivity and IoT applications,” Nat Commun, vol. 9, no. 1, 2018, doi: 10.1038/s41467-018-07632-w.

[36]. Lucchese MM et al. , “Quantifying ion-induced defects and Raman relaxation length in graphene,” Carbon N Y, vol. 48, no. 5, 2010, doi: 10.1016/j.carbon.2009.12.057.

[37]. Childres I, Jauregui LA, Park W, Caoa H, and Chena YP, “Raman spectroscopy of graphene and related materials,” in New Developments in Photon and Materials Research, 2013.

[38]. Hossain RF and Kaul AB, “Biocompatible, Inkjet Printed Heterostructure Photodetector for Biosensing Applications,” in 31st Annual Conference of the IEEE Photonics Society, IPC 2018, 2018. doi: 10.1109/IPCon.2018.8527301.

[39]. Cogan SF, “Neural stimulation and recording electrodes,” Annual Review of Biomedical Engineering, vol. 10. pp. 275–309, 2008. doi: 10.1146/annurev.bioeng.10.061807.160518.

[40]. Shao Y, Wang H, Zhang Q, and Li Y, “Fabrication of large-area and high-crystallinity photoreduced graphene oxide films via reconstructed two-dimensional multilayer structures,” NPG Asia Mater, vol. 6, no. 8, 2014, doi: 10.1038/am.2014.59.

[41]. Yagati AK, Min J, and Cho S, " Electrosynthesis of ERGO-NP Nanocomposite Films for Bioelectrocatalysis of Horseradish Peroxidase towards H 2 O 2," J Electrochem Soc, vol. 161, no. 14, 2014, doi: 10.1149/2.1001414jes.

[42]. Woods V. et al. , "Long-term recording reliability of liquid crystal polymer μ ECoG arrays," J Neural Eng, vol. 15, no. 6, 2018, doi: 10.1088/1741-2552/aae39d.

[43]. Lee WR, Im C, Koh CS, Kim JM, Shin HC, and Seo JM, "A convex-shaped, PDMS-parylene hybrid multichannel ECoG-electrode array," in Proceedings of the Annual International Conference of the IEEE Engineering in Medicine and Biology Society, EMBS, 2017. doi: 10.1109/EMBC.2017.8037018.

[44]. Michelson NJ and Kozai TDY, "Isoflurane and ketamine differentially influence spontaneous and evoked laminar electrophysiology in mouse V1," J Neurophysiol, vol. 120, no. 5, 2018, doi: 10.1152/jn.00299.2018.

[45]. Fontanini A, Spano PF, and Bower JM, "Ketamine-xylazine-induced slow (<1.5 Hz) oscillations in the rat piriform (olfactory) cortex are functionally correlated with respiration," Journal of Neuroscience, vol. 23, no. 22, 2003, doi: 10.1523/jneurosci.23-22-07993.2003.

[46]. Hwang E, McNally JM, and Choi JH, "Reduction in cortical gamma synchrony during depolarized state of slow wave activity in mice," Front Syst Neurosci, vol. 7, no. DEC, 2013, doi: 10.3389/fnsys.2013.00107.

[47]. Donaldson PD et al. , "Polymer Skulls With Integrated Transparent Electrode Arrays for Cortex-Wide Opto-Electrophysiological Recordings," Adv Healthc Mater, 2022, doi: 10.1002/adhm.202200626.

[48]. Grune C, Thamm J, Werz O, and Fischer D, "CyreneTM as an Alternative Sustainable Solvent for the Preparation of Poly(lactic-co-glycolic acid) Nanoparticles," J Pharm Sci, vol. 110, no. 2, 2021, doi: 10.1016/j.xphs.2020.11.031.

[49]. Ledochowitsch P, Olivero E, Blanche T, and Maharbiz MM, "A transparent ECoG array for simultaneous recording and optogenetic stimulation," in Proceedings of the Annual International Conference of the IEEE Engineering in Medicine and Biology Society, EMBS, 2011. doi: 10.1109/IEMBS.2011.6090808.

[50]. Kwon KY, Sirowatka B, Weber A, and Li W, "Opto-μ ECoG array: A hybrid neural interface with transparent μ ECoG electrode array and integrated LEDs for optogenetics," IEEE Trans Biomed Circuits Syst, vol. 7, no. 5, 2013, doi: 10.1109/TBCAS.2013.2282318.

[51]. Yang W. et al. , "A fully transparent, flexible PEDOT:PSS-ITO-Ag-ITO based microelectrode array for ECoG recording," Lab Chip, vol. 21, no. 6, 2021, doi: 10.1039/d0lc01123a.

[52]. Márton G, Orbán G, Kiss M, Fiáth R, Pongrácz A, and Ulbert I, "A multimodal, SU-8 - Platinum - Polyimide microelectrode array for chronic in vivo neurophysiology," PLoS One, vol. 10, no. 12, 2015, doi: 10.1371/journal.pone.0145307.

[53]. Yeager JD, Phillips DJ, Rector DM, and Bahr DF, "Characterization of flexible ECoG electrode arrays for chronic recording in awake rats," J Neurosci Methods, vol. 173, no. 2, 2008, doi: 10.1016/j.jneumeth.2008.06.024.

[54]. Vomero M. et al. , "Glassy carbon electrocorticography electrodes on Ultra-Thin and Finger-Like Polyimide Substrate: Performance evaluation based on different electrode diameters," Materials, vol. 11, no. 12, 2018, doi: 10.3390/ma11122486.

[55]. Vomero M. et al., "Achieving Ultra-Conformability with Polyimide-Based ECoG Arrays," in Proceedings of the Annual International Conference of the IEEE Engineering in Medicine and Biology Society, EMBS, 2018, vol. 2018-July. doi: 10.1109/EMBC.2018.8513171.

[56]. Renz AF et al. , "Opto-E-Dura: A Soft, Stretchable ECoG Array for Multimodal, Multiscale Neuroscience," Adv Healthc Mater, vol. 9, no. 17, 2020, doi: 10.1002/adhm.202000814.

[57]. Liang Y, Offenhäusser A, Ingebrandt S, and Mayer D, "PEDOT:PSS-Based Bioelectronic Devices for Recording and Modulation of Electrophysiological and Biochemical Cell Signals," Advanced Healthcare Materials, vol. 10, no. 11. 2021. doi: 10.1002/adhm.202100061.

[58]. Lim S, Park H, Yamamoto G, Lee C, and Suk JW, "Measurements of the electrical conductivity of monolayer graphene flakes using conductive atomic force microscopy," Nanomaterials, vol. 11, no. 10, 2021, doi: 10.3390/nano11102575.

[59]. Cui W, Lu W, Zhang Y, Lin G, Wei T, and Jiang L, “Gold nanoparticle ink suitable for electric-conductive pattern fabrication using in ink-jet printing technology,” Colloids Surf A Physicochem Eng Asp, vol. 358, no. 1–3, 2010, doi: 10.1016/j.colsurfa.2010.01.023.

[60]. Bian P, Wang Y, and McCarthy TJ, “Rediscovering Silicones: The Anomalous Water Permeability of ‘Hydrophobic’ PDMS Suggests Nanostructure and Applications in Water Purification and Anti-Icing,” Macromol Rapid Commun, vol. 42, no. 5, 2021, doi: 10.1002/marc.202000682.

[61]. Valtakari D, Liu J, Kumar V, Xu C, Toivakka M, and Saarinen JJ, “Conductivity of PEDOT:PSS on Spin-Coated and Drop Cast Nanofibrillar Cellulose Thin Films,” Nanoscale Res Lett, vol. 10, no. 1, 2015, doi: 10.1186/s11671-015-1093-y.

[62]. Stanford MG et al. , “High-Resolution Laser-Induced Graphene. Flexible Electronics beyond the Visible Limit,” ACS Appl Mater Interfaces, vol. 12, no. 9, 2020, doi: 10.1021/acsami.0c01377.

[63]. Liu Y, Dong X, and Chen P, “Biological and chemical sensors based on graphene materials,” Chem Soc Rev, vol. 41, no. 6, 2012, doi: 10.1039/c1cs15270j.

[64]. Celik N, Manivannan N, Strudwick A, and Balachandran W, “Graphene-enabled electrodes for electrocardiogram monitoring,” Nanomaterials, vol. 6, no. 9, 2016, doi: 10.3390/nano6090156.

[65]. Ozturk O. and Yapici MK, “Muscular Activity Monitoring and Surface Electromyography (sEMG) with Graphene Textiles,” in Proceedings of IEEE Sensors, Oct. 2019, vol. 2019-October. doi: 10.1109/SENSORS43011.2019.8956801.

[66]. Grijalvo S. and Díaz DD, “Graphene-based hybrid materials as promising scaffolds for peripheral nerve regeneration,” Neurochem Int, vol. 147, 2021, doi: 10.1016/j.neuint.2021.105005.

[67]. Zhu H, Liu A, Shan F, Yang W, Barrow C, and Liu J, “Direct transfer of graphene and application in low-voltage hybrid transistors,” RSC Adv, vol. 7, no. 4, 2017, doi: 10.1039/c6ra26452b.

[68]. Lambert BJ and Tang FW, “Rationale for practical medical device accelerated aging programs in AAMI TIR 17,” in Radiation Physics and Chemistry, 2000, vol. 57, no. 3–6. doi: 10.1016/S0969-806X(99)00403-X.

[69]. Rynes ML et al. , “Assembly and operation of an open-source, computer numerical controlled (CNC) robot for performing cranial microsurgical procedures,” Nat Protoc, vol. 15, no. 6, 2020, doi: 10.1038/s41596-020-0318-4.

[70]. Bernhard SM et al. , “An automated homecage system for multiwhisker detection and discrimination learning in mice,” PLoS One, vol. 15, no. 12 December, 2020, doi: 10.1371/journal.pone.0232916.

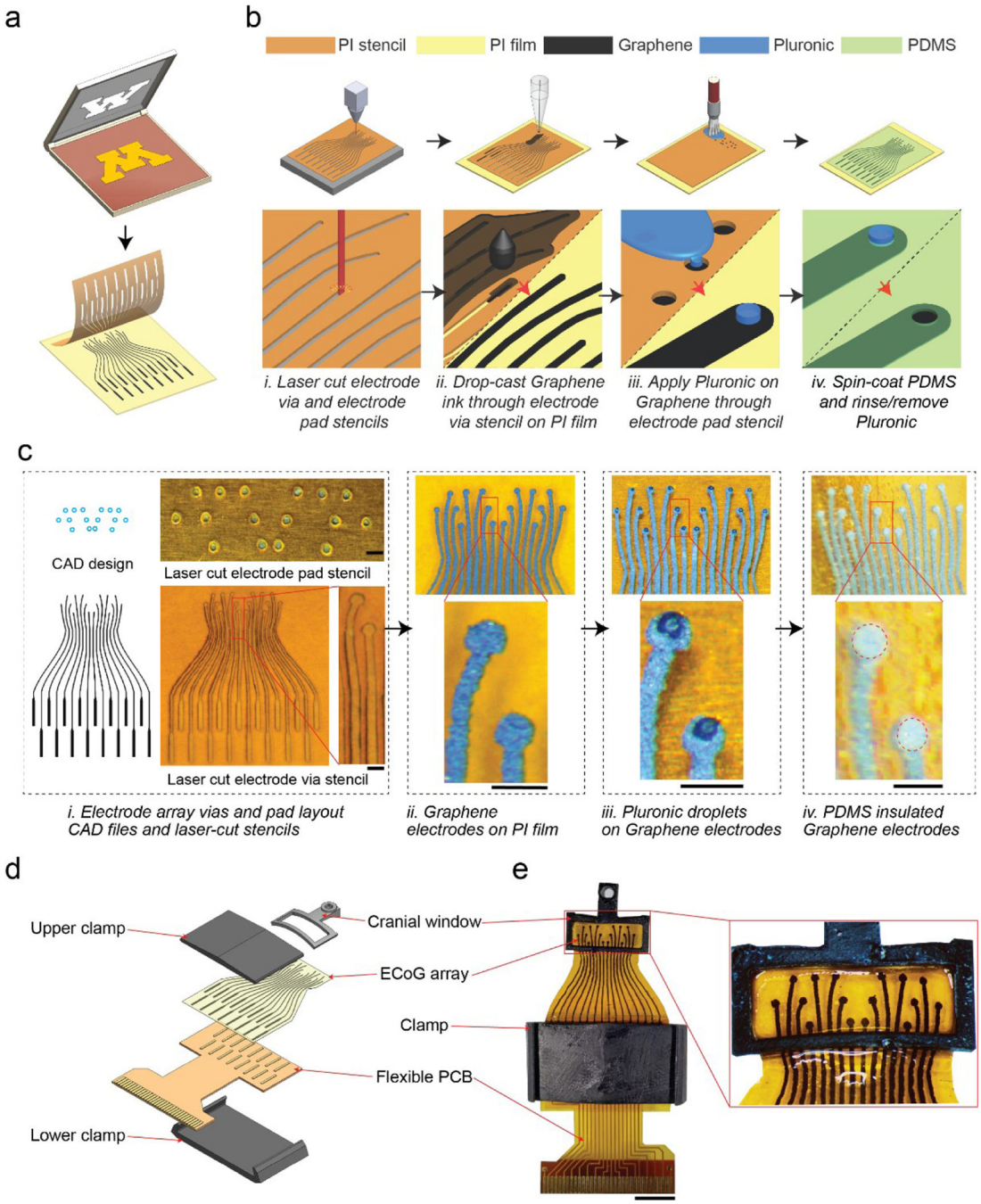

Figure 1 |. Stencil-printed flexible graphene ECoG array:

(a) Stencil-printing adapted from screen-printing to flexible neural interfaces. **(b)** Schematic of the graphene ECoG electrode array fabrication procedure. (i) Stencils are cut from insulating polyimide tape (PI) using a desktop laser; (ii) After tape-transferring the stencil onto a PI film, graphene ink was drop-cast via stencil on the PI film to pattern the electrode traces, followed by annealing; (iii) After removing the electrode stencil from the PI film, Pluronic sacrificial layer is deposited through the electrode pad stencil on the graphene electrodes; (iv) Once the Pluronic layer solidifies, the electrode pad stencil is carefully

removed from the graphene electrode array. Diluted PDMS is spin coated to form the insulating layer. After the PDMS cures, the Pluronic layer is rinsed away to expose the electrode pads. **(c)** (i) Computer-aided design (CAD) drawing and images of laser-cut stencils for electrode array vias and electrode pads. (ii) The patterned graphene electrode on PI film. (iii) Pluronic droplets on graphene electrodes. (iv) PDMS insulated graphene electrodes. Scale bars indicate 500 μm. **(d)** CAD rendering of the whole implant assembly. The PDMS-insulated graphene ECoG electrode array is first bonded to a flexible PCB using silver epoxy adhesive to connect the ECoG array with the PCB's gold pads. The bonded PCB and ECoG array are mechanically reinforced by a 3D printed clamp. **(e)** Photograph of a fully assembled 16-channel graphene ECoG device. Scale bar indicates 5 mm.

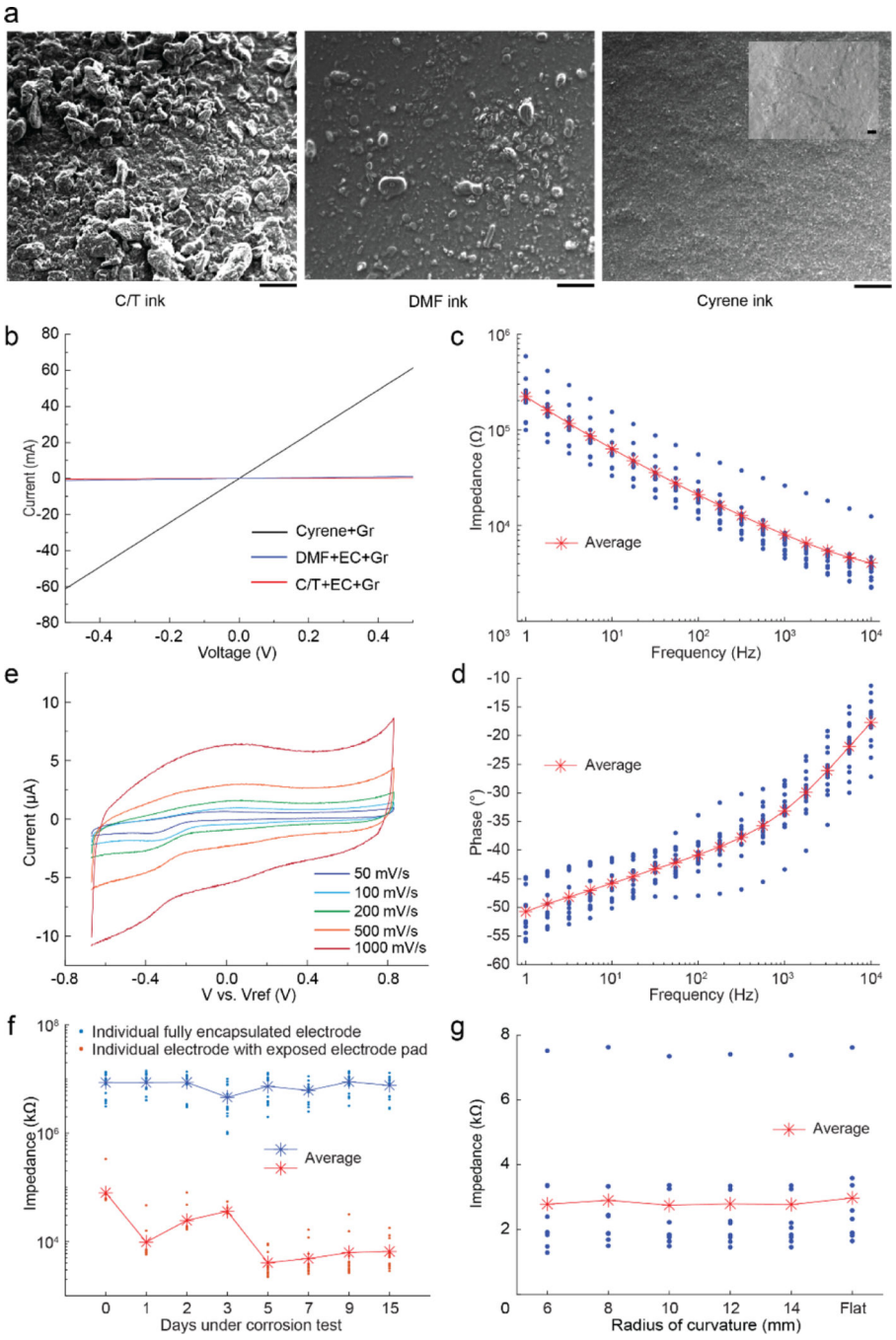

Figure 2 |. Material characterization of graphene films using three graphene inks and electrochemical characterization of graphene ECoG electrodes:

(a) SEM images of the surface morphology of graphene films drop-cast onto a SiO_2/Si substrate. The inset in the top right image shows the higher magnification image. Scale bars indicate 200 μm, while the scale bar in the inset indicates 2 μm. **(b)** Current-voltage characteristics of three exfoliated graphene inks: graphene exfoliated in Cyrene (Cyrene+Gr), graphene exfoliated in Dimethylformamide with Ethyl Cellulose (DMF+EC+Gr), and graphene exfoliated in a mixture of Cyclohexanone and Terpineol with

Ethyl Cellulose (C/T+EC+Gr). **(c)** Impedance magnitude, at frequencies ranging from 1 Hz to 10 kHz of ECoG electrodes made by stencil printing with Cyrene + graphene ink. **(d)** Phase angle at different frequencies ranging from 1 Hz to 10 kHz made by stencil printing with Cyrene + graphene ink. **(e)** Cyclic voltammetry of the graphene ECoG electrode in 1X PBS at different scan rates from 50 to 1000 $mV \cdot s^{-1}$. **(f)** Change in impedance magnitude as a function of time during an accelerated corrosion test. Each device has 16 electrodes with exposed electrode pads (red) and 16 electrodes with PDMS capsulated pads (blue). **(g)** The change of impedance magnitudes at 1 kHz as a function of radii of bending curvature for nine identical, 10 mm long, straight, graphene ECoG electrodes.

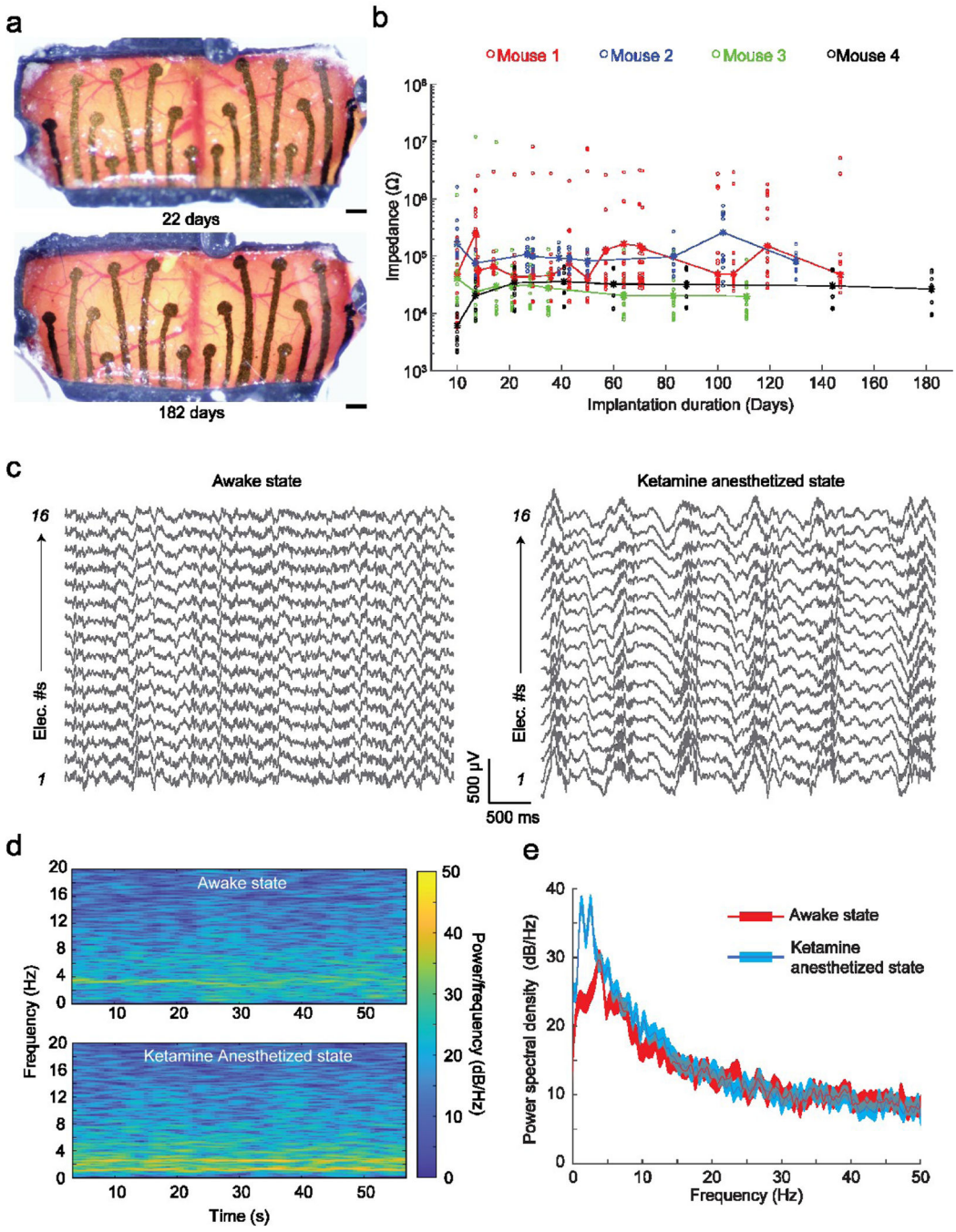

Figure 3 |. *In vivo* performance of the graphene ECoG devices:
(a) Optical microscope images taken at 2 timepoints after chronic implantation of ECoG device on a C57BL/6 mouse (Mouse #4 shown in **(b)**). Scale bars indicate 500 μm. (**b)** Impedance magnitude at 1 kHz of 64 electrodes in 4 implanted mice. Dots indicate individual electrode impedance values. Stars indicate the average impedance of the 16 electrodes in each device. **(c)** Raw surface field potential recordings from the electrodes in awake and Ketamine anesthetized states. **(d)** Frequency spectrogram of electrode 5 shown in

(c) in awake and anesthetized states. **(e)** Average power spectral density (PSD) of recordings of all electrodes shown in **(c)** in awake and anesthetized states.

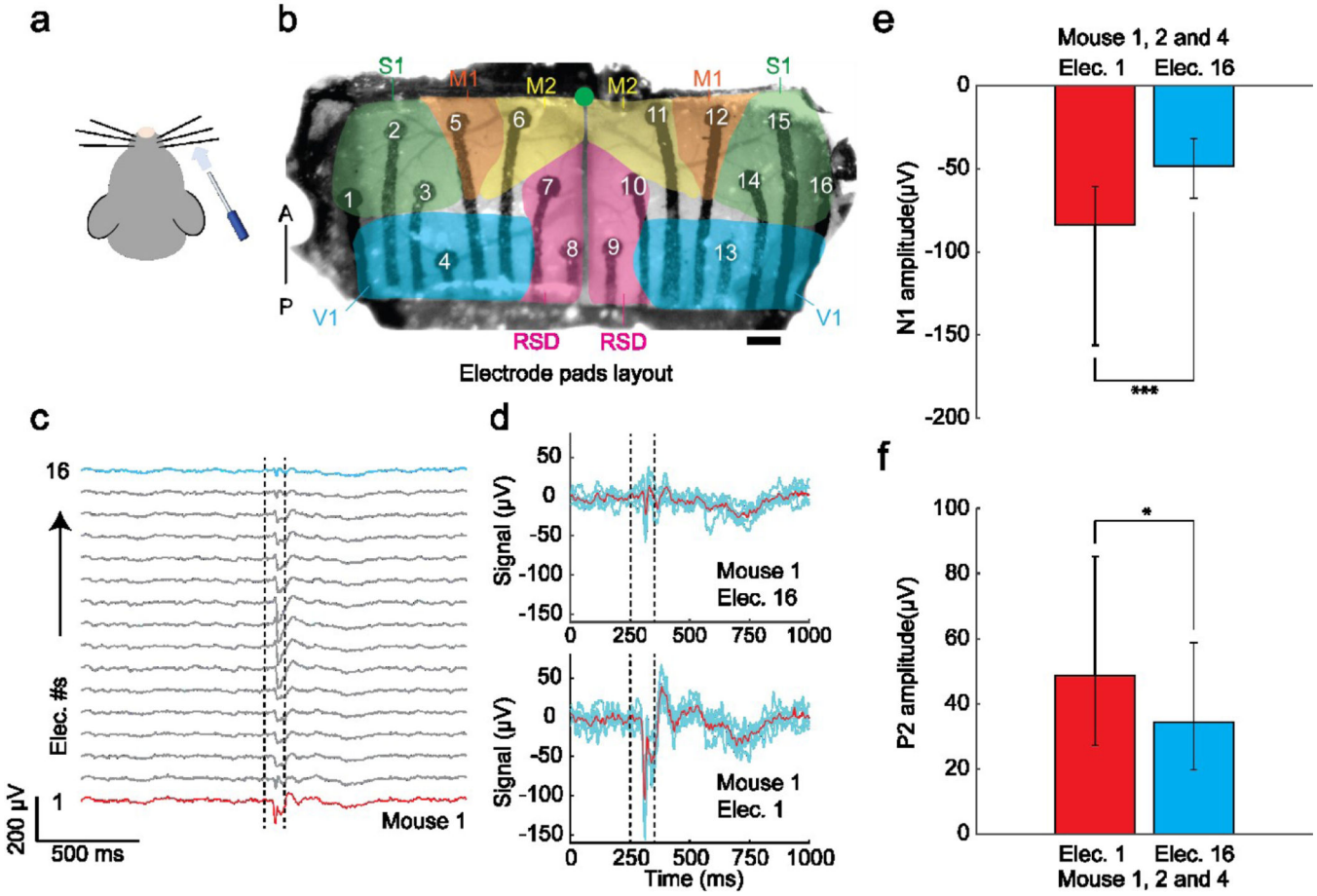

Figure 4 |. Sensory stimulus-evoked responses recorded by the graphene ECoG devices.

(a) Air puff stimulus was applied to the right whiskers. **(b)** Locations of electrode pads: electrodes 1 – 3 and 14 – 16 were located in the primary sensory cortex (S1); electrodes 4 and 13 were located in the visual cortex (V1); electrodes 5, 6, 11, and 12 were located in the primary motor cortex (M1/M2); electrodes 7, 8, 9, and 10 were located in the Retrosplenial cortex (RSD). Green dot indicates Bregma. Scale bar indicates 500 μm. **(c)** Average ECoG signals responses to air-puff stimuli (n = 138) in 20-min recording were collected from 16 electrodes of Mouse #1. Dotted lines indicate the on- and off-state of the air puff stimulus. Red line marks the signal of contralateral electrode 1, and blue line marks the signal of ipsilateral electrode 16 **(d)** Average ECoG signals captured by the contralateral electrode 1 (top) and ipsilateral electrode 16 (bottom) in response to repeated whisker stimulus (n = 5) in Mouse #1. Blue lines indicate individual trials. Red line denotes the average signal response. **(e)** Comparison of surface field potential of depolarization's peak amplitudes recorded by the contralateral electrode 1 vs. ipsilateral electrode 16 on mice 1, 2, and 4 ($P < 0.001$, *t-test*). **(f)** Comparison of local field potential repolarization's peak amplitudes recorded by the contralateral electrode 1 vs. ipsilateral electrode 16 of the graphene ECoG on mice 1, 2, and 4 ($P < 0.01$, *t-test*).